

# Improvements in Mechanical Properties of Spring Steel Through Surface Tempering and Hardening Assisted by SMAT

Prashant Tadge<sup>1</sup> · C. Sasikumar<sup>1</sup>

Received: 9 August 2017 / Accepted: 30 January 2018 / Published online: 21 February 2018  
© The Indian Institute of Metals - IIM 2018

**Abstract** In this paper, the microstructural, mechanical properties of hardened and tempered spring steel altered by surface mechanical attrition treatment (SMAT) were investigated. The effect of SMAT on surface microstructure, phase constituents, hardness, elastic and plastic properties of the surface: Young's Modulus, stiffness, YS, UTS were analyzed. The SMAT was carried out for different time periods such as 15, 30, 45, 60 and 75 min respectively. SMAT introduced severe plastic deformation (SPD) over the surface with case depth of about 200–300  $\mu\text{m}$ . The SEM microstructure revealed the presence of tempered lath martensite in as received samples while SMAT had resulted in the formation of twinned martensite at SPD regions. Further, it was also found that fine carbides ( $\text{Fe}_3\text{C}$ ) started to precipitate and led to the formation of alternate layers of tempered martensite and  $\text{Fe}_3\text{C}$  indicating stress relaxation/tempering by SMAT. The X-ray and EDX results also confirmed the presence of martensite in as received samples and precipitation of carbides by SMAT. However, in contrast to a thermal tempering, the surface hardness was found to be increasing due to the effects of SPD. The SMAT had altered the mechanical properties of the steel significantly. The stiffness of the leaf spring was 1452 and 2032  $\text{N mm}^{-1}$  respectively for the samples before and after 15 min of SMAT. This could be attributed to the resistance to elastic deformation caused by surface composite layer. It was also interesting to note that the toughness of the hardened and

tempered spring steel increased from  $242.45 \times 10^4$  to  $337.12 \times 10^4 \text{ J m}^{-3}$  by 75 min of SMAT.

**Keywords** Mechanically induced tempering · Surface mechanical attrition treatment · Severe plastic deformation · Mechanical properties · Spring steel

## 1 Introduction

Hall [1] and Petch [2] demonstrated increased strength of metals and alloys with finer grains. This concept had attracted the attention of researchers and scientists working on nano-crystalline materials to develop ultra high strength materials. However, the nano-structured metals exhibited inverse Hall–Petch effect below certain critical size [3], while the fracture toughness and the possibility of super-plastic deformation improved significantly. Appreciable changes were also noticed in functional properties of materials such as electrochemical behavior, diffusivity, surface absorption of hydrogen etc. Pedneault et al. [4] had produced a nano-structured metal hydride by cold rolling and demonstrated superior electrochemical properties. Zhang et al. [5] and other researchers [6, 7] showed improved hydrogen absorption of Ti and Mg alloys produced by a nano-crystallization technique. In fact the nano-crystalline materials showed fundamentally different properties from bulk materials which found potentially important technological applications [8–10].

Over the past decade, researchers had developed many severe plastic deformation (SPD) processes [11–16] such as equal channel angular pressing (ECAP), high pressure torsion (HPT), cyclic close die forging (CCDF), repetitive corrugations and straightening (RCS) and multi directional

✉ Prashant Tadge  
prashant\_tadge@rediffmail.com

<sup>1</sup> Department of Materials and Metallurgical Engineering,  
Maulana Azad National Institute of Technology, Bhopal  
462003, India

forging (MDF) to produce industrial scale nano-materials. In most engineering alloys and designs it is required to modify the surface properties rather than the bulk properties of the materials. Lu and Lu [3] had introduced the concept of surface nano-crystallization (SNC) through surface mechanical attrition technique (SMAT) on metallic materials. The pioneering work of Lu and Lu and others demonstrated the potential of SMAT in producing a nanocrystalline surface and thereby modifying the surface properties of metals and alloys [3, 17, 18]. The surface mechanical attrition treatment (SMAT) is similar to the conventional shot peening process, where the metal surface is subjected to continuous bombardment with fast moving steel/cast iron/ceramic balls; thereby severe plastic deformation is induced over the surface. This in turn causes increased dislocation density and mechanical twins over the surface of the metals. Tao et al. [19] had carried out a detailed investigation on the dislocation structures and formation of grain/sub-grain boundaries by SMAT. The authors studied the movement and arrangement of dislocations as dense dislocation walls (DDW) during severe plastic deformation process. In due course, ultrafine and nano-crystalline surface consisting of enhanced grain boundaries was produced. Many research publications showed the possibility of producing about 10–20 nm crystals by SMA treatment for over 30–60 min depending on the process parameters. Further, it was also noted that SMAT produced a layered structure due to the arrangement of dislocation networks as discussed by Tao et al. [20, 21]. In fact, this was considered as a composite structure consisting of crystalline and amorphous layer (grain boundary) of the same material. In dispersion hardened materials and dual phase alloys, these layers consisted of alternate layers of soft and hard phases apart from amorphous grain boundary region [22]. This type of micro-structural arrangement besides the size effect altered the mechanical properties of the materials significantly.

The interesting works of Chen et al. [23] demonstrated the possibility of designing micro-mechanical devices with ultra-high strength metals and alloys by SMAT. The authors showed that the yield strength of stainless steel rose from 250 to 1450 MPa by SMAT and also proved that the significant change was due to the effect of SMAT and not by the possible martensitic transformation during severe plastic deformation. Many other researchers [24–27] also showed a marginal rise in the mechanical properties of materials, however most these studies pertained to pure metals and alloys having higher ductility. There are very few reports on SMAT of hardened and tempered materials while the surface nano-crystallization (SNC) has a potential for producing a surface with an unusual combination of hardness and toughness.

The residual compressive stresses stored over the material's surface contributed significantly to improving inherent tendency of the material for resisting the crack propagation. The compressive residual stress in conventional shot peening was about 500–600 MPa while it was more than 800 MPa in SMAT process. The strain induced by SMAT process was in the range of 0.01–0.08 which was much lower than any other SPD techniques [28–31]. Sara Bagherifrad [32] and other researchers [33, 34] had shown that the conventional shot peening rose the fatigue life of low alloy steel by 3% while the same was raised by 13% by SMAT. The attempt made by Vielma and co-workers [33] on hardened and tempered steel proved three times rise in fatigue life. However, there is only little work on SMAT of hardened steel used in most engineering applications and it requires many studies. In the present work the effect of SMAT on hardened and tempered steel used for making leaf spring has been investigated.

## 2 Experimental Procedures

### 2.1 Materials and Method

A commercial spring steel AISI6150 with composition of 0.48C, 0.86Mn, 0.81Cr, 0.7Ni, 0.27Si, 0.12 V (in wt%), and rest Fe was used for the investigation. The material was obtained in hardened and tempered condition. The samples to be treated were cut into 150x20x8 mm and placed in the equipment used for SMAT as shown in Fig. 1. The equipment had a chamber in which stainless steel shots of 3 mm diameter were filled. An electrical



**Fig. 1** Experimental set-up used for surface mechanical attrition treatment of AISI 6150 steel

controlled vibrator fixed at the bottom of the chamber was made to vibrate at a frequency of 180 Hz. The working distance between the vibrator and the sample was about 260 mm. By this action, the stainless steel shots were made to collide continuously on the sample surface. The process was carried out for 15, 30, 45, 60, 75 min respectively. The treatment was repeated on all sides of the sample. 400 g of balls were used and the operation was carried out at room temperature. The frequency, ball velocity, ball size and working distance were maintained constant for all the experiments. In order to avoid overheating, the process was stopped at regular intervals and allowed for cooling.

## 2.2 Characterization Techniques

The microstructures of the samples before and after SMAT were investigated using a JEOL 6390 scanning electron microscopy (SEM) facilitated with energy dispersive spectroscopic analysis (EDS). Any phase change during the process was investigated using Bruker AXE D2 Phaser with Cu target in the range of 20°–90°. The yield behavior, tensile strength, plastic deformation characteristics and toughness were investigated with a Universal Testing Machine (Mechatronic, India). The Young's Modulus, spring constant and the surface hardness of the steel was investigated by using three-point bend test and Micro-Vicker Hardness Tester (HM-210/220B) respectively.

## 3 Results and Discussions

### 3.1 Thickness of SMATed Region

Figure 2 shows the typical cross-sectional image of surface mechanical attrition treated sample for 15 min. As shown,



**Fig. 2** Microstructure of SMATed sample reveals the thickness of severe plastic deformed region

the severe plastic deformed region is found to vary in the range of 200–300 μm depending upon the process time.

### 3.2 XRD Analysis

The typical X-ray diffractogram of the samples subjected to SMAT for 0, 15, 45 and 60 min are shown in Fig. 3. The inset shows enlarged view of the major peak. The XRD results confirm the presence of body centered tetragonal (BCT) martensitic peaks (ICDD-00/044/1290) with reflections of (101), (110), (200) and (211) at 44.183, 44.803, 65.222 and 80.842 respectively.

The martensitic peak of as received sample is broad indicating microstrain of the lattice. The intensity of the peaks is found to increase with process time depicting the relaxation of microstrain.

Further, it is also noticed that the Fe<sub>3</sub>C peaks are found to be separating out from martensitic peaks confirming the relaxation process. The carbon content of martensite is derived using the method established by Robert [35]. The relations between lattice parameter and carbon content are given below

$$c = 2.861 + 0.116m \quad (1)$$

$$a = 2.861 - 0.013m \quad (2)$$

The above mentioned equation can be rearranged to calculate the peak shift induced by carbon content.

$$\Delta(\overline{2\theta}) = 2 \left[ \sin^{-1} \left( \frac{\lambda}{a} \right) \right] - 2 \left[ \sin^{-1} \left( \frac{\lambda}{c} \right) \right] \quad (3)$$

where, a and c are lattice parameters, m is carbon content,  $\Delta(\overline{2\theta})$  is the shift in angle of diffraction due to carbon content and  $\lambda$  is wavelength of X-ray. The variation of the surface carbon content of martensite determined using Eq. 3 is shown in Fig. 4. The carbon content decreases with process time confirming the stress relieving process.

### 3.3 SEM Analysis

The SEM images of the samples before and after SMA treatment are delineated in Fig. 5a–d for various time periods. The microstructure reveals the presence of tempered lath martensite in as received sample. After SMAT treatment, layering of martensitic structure on the surface is observed. Close observation of the microstructure has indicated the presence of alternate layers of martensite and carbides. The EDS spectra of the sample have been used to show the presence of iron, carbon and other elements present in the material at affected regions introduced by SMAT shown in Fig. 6. With the SMAT of 15 min, the plate martensite is formed which is shown in Fig. 5b and then it is transformed into lath martensite shown in Fig. 5c

**Fig. 3** XRD patterns of spring steel AISI 6150 before and after SMAT

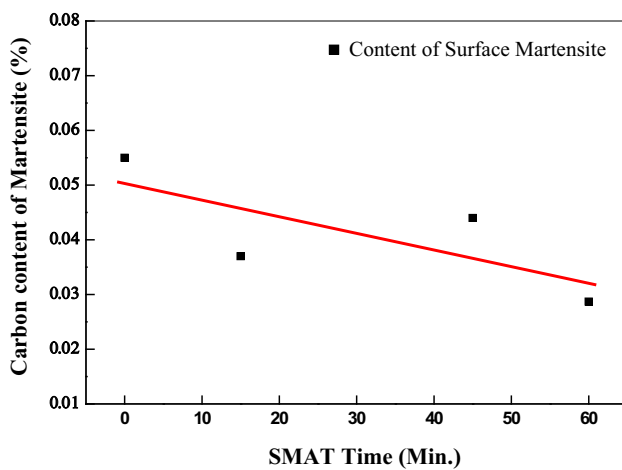
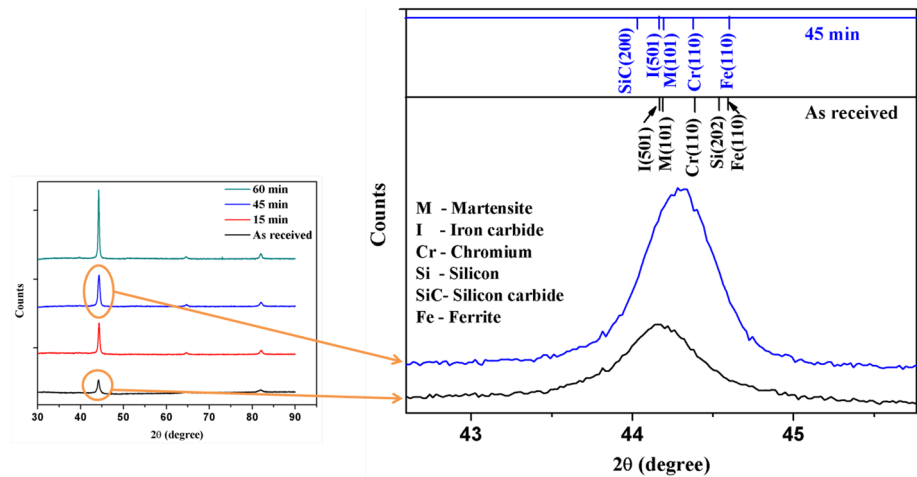


**Fig. 4** Variation of surface carbon content of mechanically tempered martensite

and d. The enlarged view of lath martensite is shown in the inset view (Fig. 5b). A similar study has been reported by [24, 36] indicating that these kind of structures can be related to twinned related laths.

Severe plastic deformation introduced by SMAT has resulted in the formation of layered structure due to the movement of dislocation. Thereby the microstructure transforms into a layered structure as shown in the schematic illustration (Fig. 7). Similar observation has also been reported in ferritic or austenitic steel subjected to severe plastic deformation [19]. Further, it is also noticed that SMAT has led to the precipitation of carbides as that of tempering treatments. The carbide precipitation found to have increased with treatment time. After 75 min of treatment, maximum amount of carbides are precipitated in the martensitic matrix.

The strengthening due to SMAT can be attributed to hardening by dispersant, sub grain boundaries and dislocation hardening. The dispersant hardening of the present

sample is due to the precipitation of carbides from a supersaturated solid solution of martensite. The Orowan stress [37]  $\sigma_{or}$  can be written as below

$$\sigma_{or} = \frac{0.8MGb}{\lambda} \quad (4)$$

where, M is the Taylor factor (= 3), G is the shear modulus, b is the magnitude of the Burgers vector and  $\lambda$  is the mean interparticle spacing. The mean interparticle spacing  $\lambda$  is found to increase with time of SMAT.

It is also noticed that SMAT creates laths or block boundaries resulting in sub boundary hardening. The hardening by Lath or sub boundary [37] is given as

$$\sigma_{LT} = \frac{10Gb}{\lambda_{LT}} \quad (5)$$

where,  $\lambda_{LT}$  is the shortest lath thickness in the martensitic matrix and is in the range of 0.2–0.8  $\mu\text{m}$ .

SMAT also shows significant change in the laths' thickness of martensitic structure, the variation of the thickness of laths with different processing time is reported in Fig. 9. As shown in Fig. 8a–c, the thickness of lath decreases from 540 to 220 nm by 45 min of SMAT treatment. Thus SMAT lead to the formation of fine layers of martensite and carbides. However, further processing, produces the carbide particulates in the matrix which show the effect in hardness discussed in a later section.

The dislocation density hardening [37] is an important strengthening mechanism in steel and can be written as

$$\sigma_p = 0.5MGb(\rho_f)^{1/2} \quad (6)$$

where,  $\rho_f$  is the free dislocation density in the matrix. However, in most reports, the dislocation density decreases by nanocrystallization.

During SMAT, twin boundaries are created due to severe plastic deformation. The spacing between twin boundaries is found to decrease as SMATing time increases



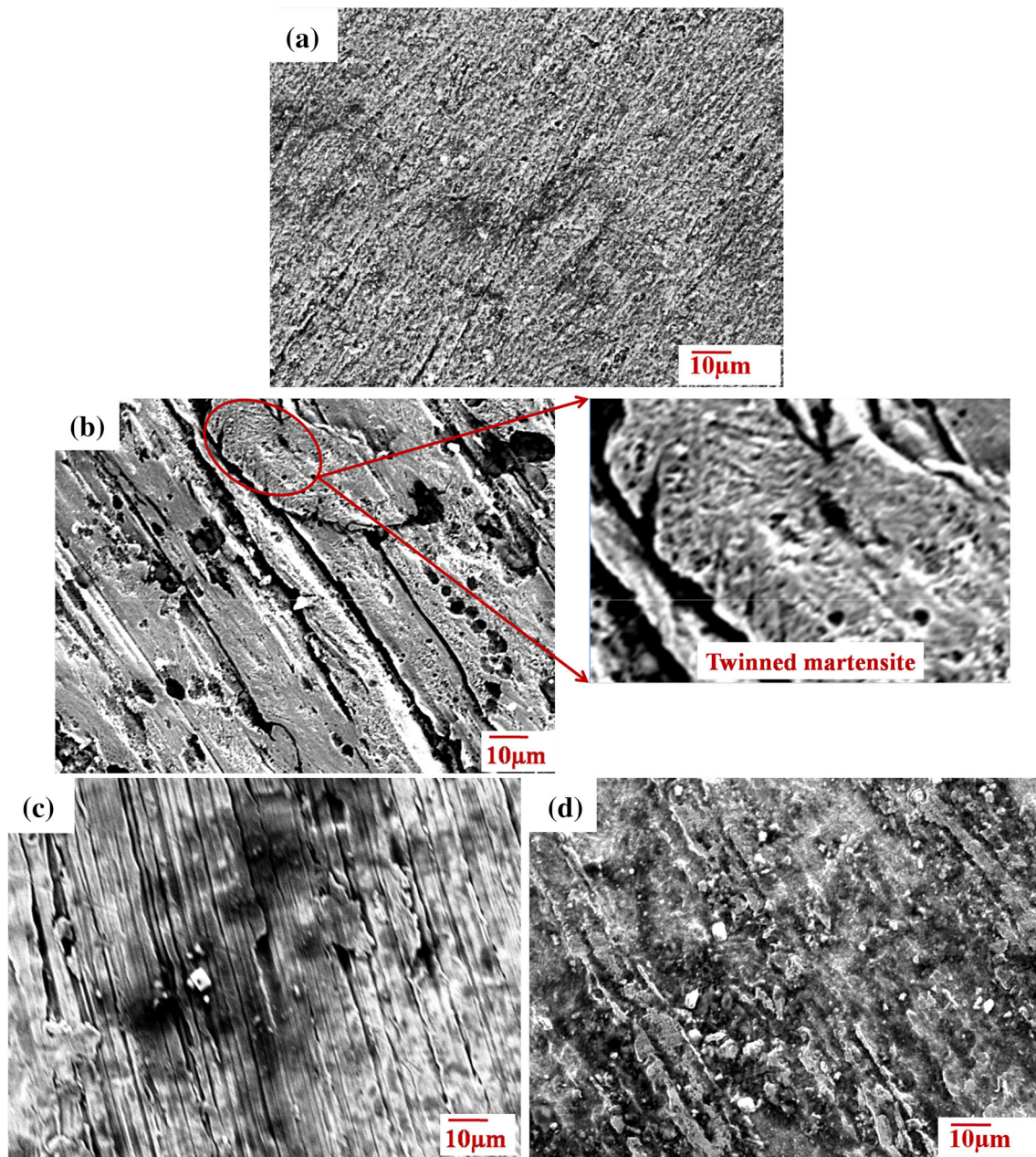


**Fig. 5** SEM images illustrating the microstructural changes at **a** 0 min, **b** 15 min, **c** 45 min, **d** 60 min of SMA Treatment

i.e. the interlamellar spacing decreases with process time as shown in Fig. 8a–c. It is also found that fine carbides segregate along the twin. This process occurs up to 45 min of SMAT beyond which the matrix become softer and no carbides segregate. On further processing, the intermixing of carbides and matrix occur which produces the spherical particulates and the carbide particles are dispersed throughout the matrix instead of producing fibrous carbide layer.

### 3.4 Mechanical Properties

The tensile behavior of the AISI 6150 spring steel in as received condition and after SMAT are illustrated in Fig. 10.

The yield strength, ultimate tensile strength, toughness and strain hardening behavior altered by SMAT are evaluated and discussed below. The Young's Modulus and spring constant evaluated using bending test are also reported.

Fig. 6 EDS spectra peaks

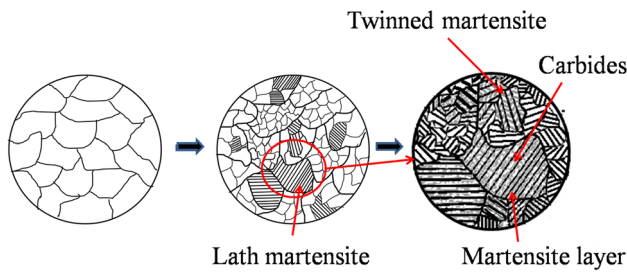
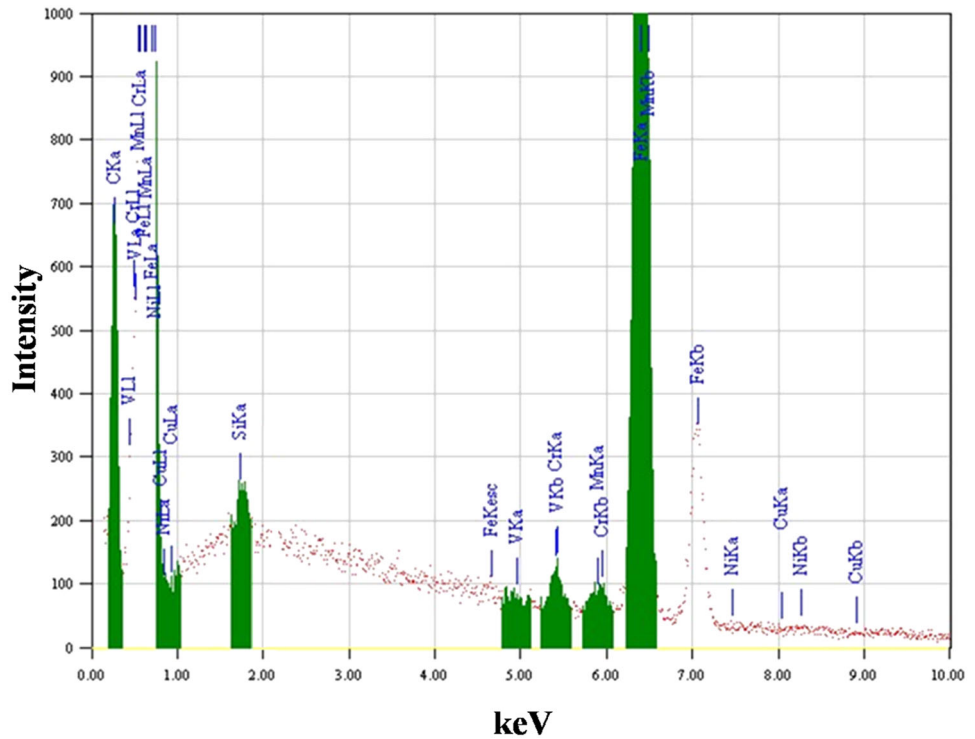


Fig. 7 Schematic illustration of depicting the formation of layered structure by SMAT

3.4.1 Young’s Modulus and Spring Constant of SMATed Spring Steel

The variation of Young’s Modulus (E) with time of SMAT is shown in Fig. 11. The value of E increases by about 40% by 15 min of SMAT. The value is found to decrease beyond 15 min of SMAT. The increase in E can be attributed to compressive residual stress over the surface. The high modulus can be attributed to the compressive stress and the SMAT reduces equilibrium spacing between the atoms leading to larger elastic modulus. The Young’s Modulus for a material can be written as

$$Y = \frac{F/A}{\delta X/X} = \frac{F/y^2}{\delta X/r_0} \cong \frac{dF}{dr} \frac{r_0}{y^2} \tag{7}$$

where,  $r_0$  and  $y$  are inter-atomic separations of the atoms in longitudinal and transverse directions,  $y^2$  is the area of

element. The force ( $dF/dr$ ) is the summation of attractive and repulsive forces between the atoms. The SMAT leads to increase in the value of Young’s Modulus by optimum combination of attractive and repulsive forces.

The decrease in the modulus of elasticity after 15 min of SMAT can be attributed to the surface porosity introduced by the process. Using the method of Coble and Kingery [38], the relation between Young’s Modulus and porosity can be written as

$$E_f = E (1 - P) \tag{8}$$

where,  $E_f$  is the effective Young’s Modulus of porous material,  $E$  is the Young’s Modulus of solid material and  $P$  is the porosity in the material. With the time of SMAT, the porosity increases and it leads to decrease in the value of Young’s Modulus in the material. The porosity in the surface can be seen in Fig. 5.

The Young’s Modulus and stiffness of the material can be determined by the three-point bending test. The relation between Young’s Modulus and deflection can be written as

$$E = \frac{FL^3}{48I\delta} \tag{9}$$

where,  $E$  is the Young’s Modulus,  $F$  is the applied force,  $L$  is the span length,  $\delta$  is the deflection and  $I$  is the inertia factor and can be written as

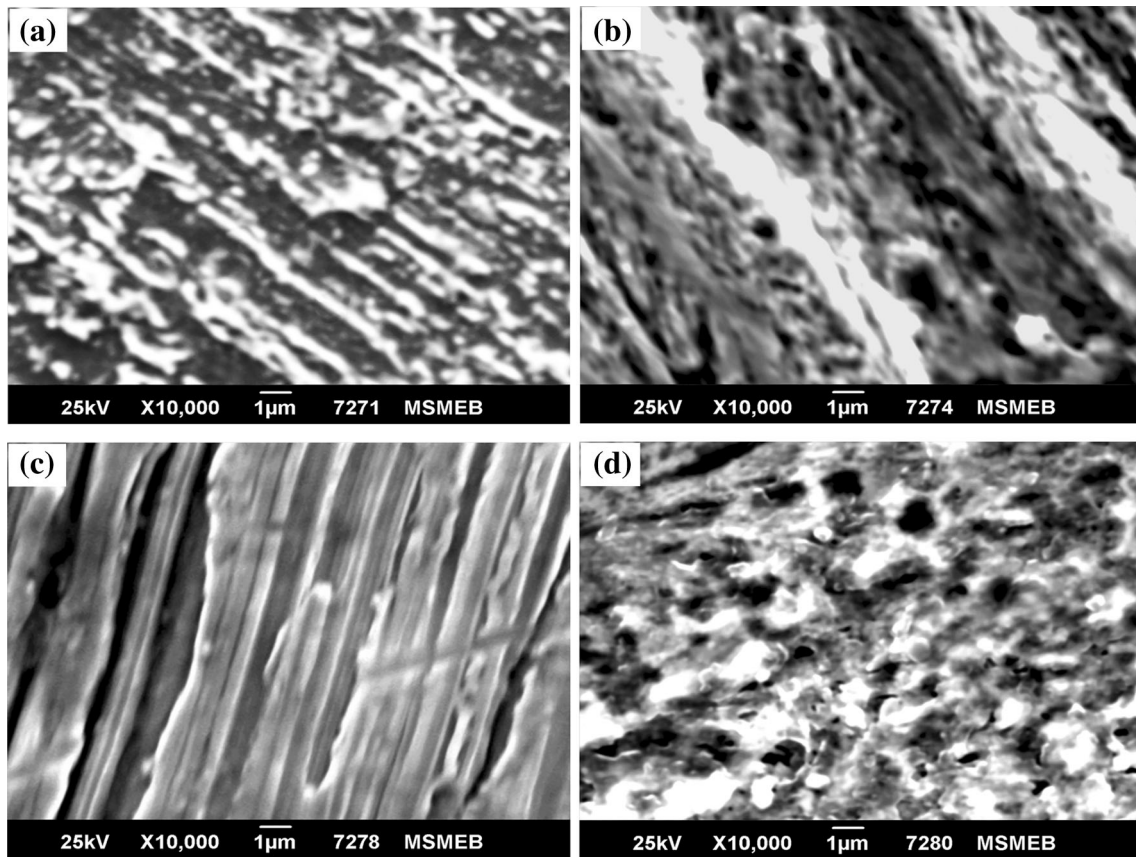


Fig. 8 SEM images at higher magnification for a 0 min, b 15 min, c 45 min, d 60 min SMA Treatment

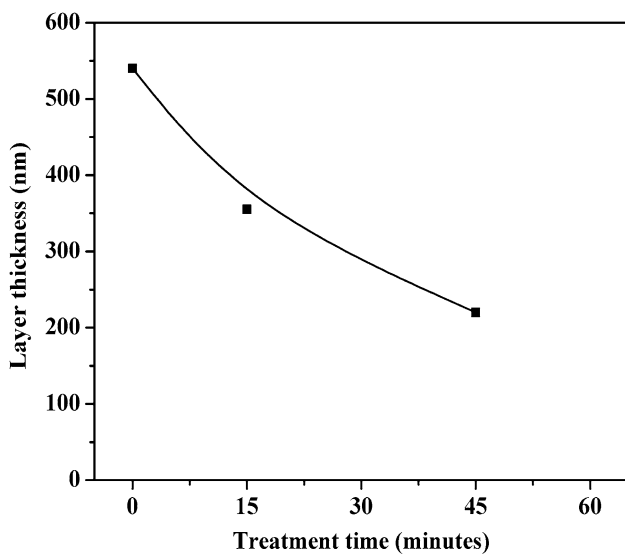


Fig. 9 Variation of layer thickness of laths with SMA treatment time

$$I = \frac{bh^3}{12} \tag{10}$$

where, b & h are the width and height of the material. The spring constant or stiffness of the material can be

determined by the slope of applied force and deflection which can be written as

$$Stiffness(k) = \frac{F}{\delta} \tag{11}$$

### 3.4.2 Variation of Yield Strength

The yield strength is found to increase exponentially with time. The variation of yield strength is shown in Fig. 12. This variation can be due to the strengthening of the crystals by carbide precipitation and formation of sub grains boundaries. Yield strength has increased by about 17% in comparison to a conventional quench hardening and tempering technique.

### 3.4.3 UTS and Plastic Deformation Behavior

The maximum load bearing of the materials also increases with SMAT. The strain hardening coefficient of the material is calculated by true stress true strain relationship as given in Fig. 13.

The strain hardening coefficient decreases with SMAT indicating that the plastic stress required for deformation is decreasing. This result suggests that the material is



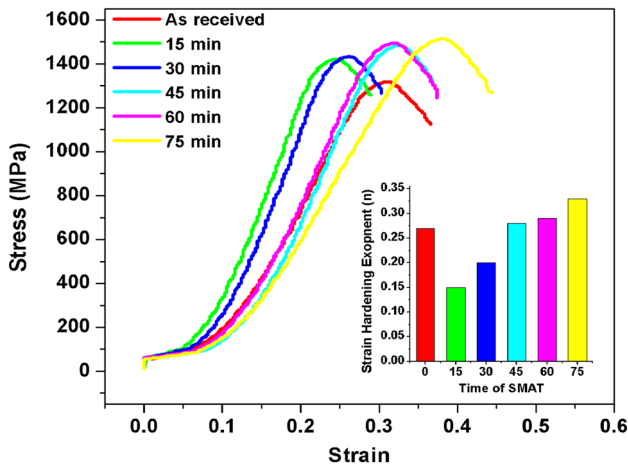


Fig. 10 Tensile behavior of hardened and tempered martensite by SMAT

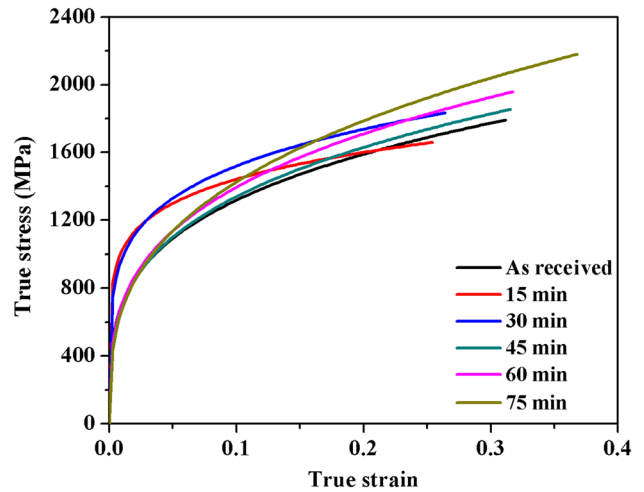


Fig. 13 Variation of true stress with true strain

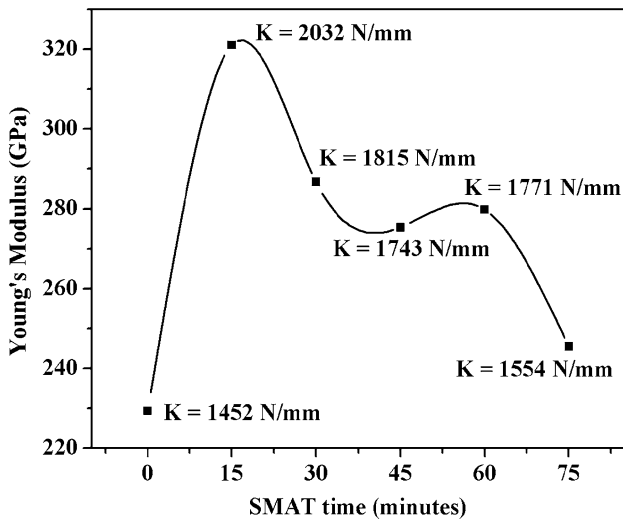


Fig. 11 Variation of Young's Modulus (E) and stiffness with SMAT time

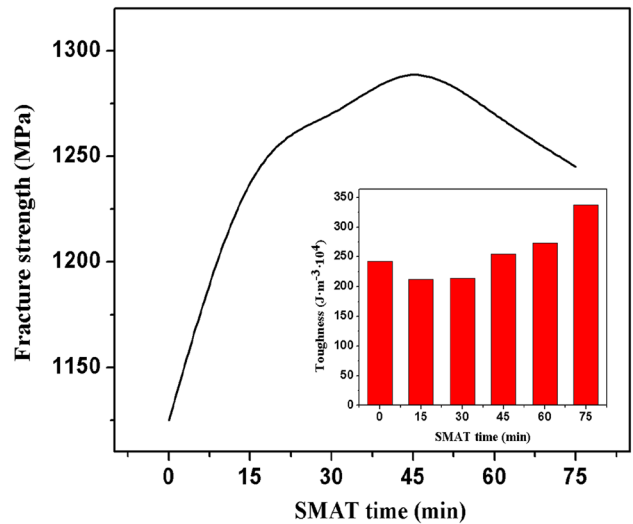


Fig. 14 Variation of fracture strength and toughness with SMAT time

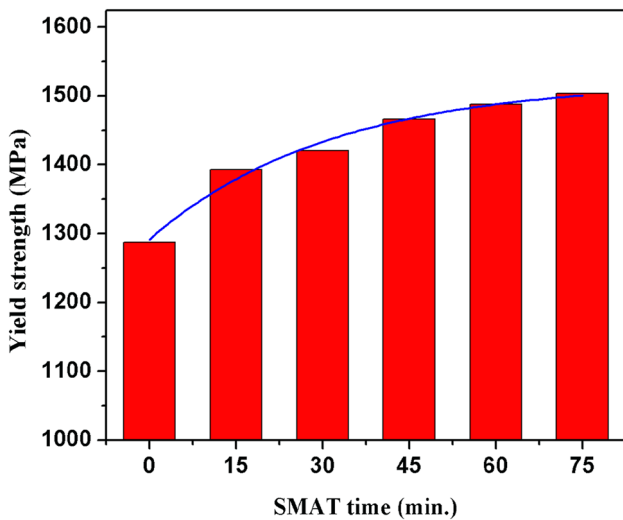


Fig. 12 Variation in yield strength with SMAT time

softened by SMAT in addition to the strengthening caused by another effect i.e. the change in plastic deformation characteristic are the summation of the strengthening and weakening effect. The weakening effect is due to the fact that nano grains are not able to stabilize the dislocations; thereby the dislocation densities are decreasing. Thus the strain hardening coefficient of the material decreases with the time of SMAT. The plastic strain also decreases with SMAT while the elastic strain component increases. This can be attributed to interatomic forces between the atoms.

### 3.4.4 Fracture Strength and Toughness

The fracture strength of the material is slightly increased by SMAT as illustrated in Fig. 14. This is due to the fact that the neck formed after UTS grows at a slower rate in



comparison to as received material. This result also suggests that the material offers increased resistance for crack propagation. The compressive residual stress provides the resistance for crack propagation. In general, the quenched and hardened steel shows poor toughness. However, interestingly the toughness of the material increases by SMAT treatment, i.e. the material is able to store plastic strain energy without cracking. The toughness is the ability to absorb mechanical energy up to the point of failure and can be determined as

$$\frac{\text{Energy}}{\text{volume}} = \int_0^{\varepsilon_f} \sigma d\varepsilon = U_T \quad (9)$$

Where,  $\sigma$  is the stress,  $\varepsilon$  is the strain,  $\varepsilon_f$  is the strain upon failure and  $U_T$  is the toughness. The reduction in area for as quenched and hardened sample is  $242.45 \times 10^4 \text{ J m}^{-3}$  and that of SMATed is  $337.12 \times 10^4 \text{ J m}^{-3}$ . The current investigation shows that in a spring steel, the increase of Young's Modulus toughness by around 40% can be produced by SMAT.

#### 3.4.5 Effect of SMAT on Surface Hardness

Variation of surface hardness of samples subjected to SMAT for different time periods is shown in Fig. 15. The received sample shows the hardness of 400HV<sub>0.2</sub> while the SMAT treated samples show increased surface hardness of about 600HV<sub>0.2</sub>. After initial 15 min of treatment, the hardness decreases slightly as the carbide precipitation occurs. A considerable change in hardness is observed after 60 min of treatment.

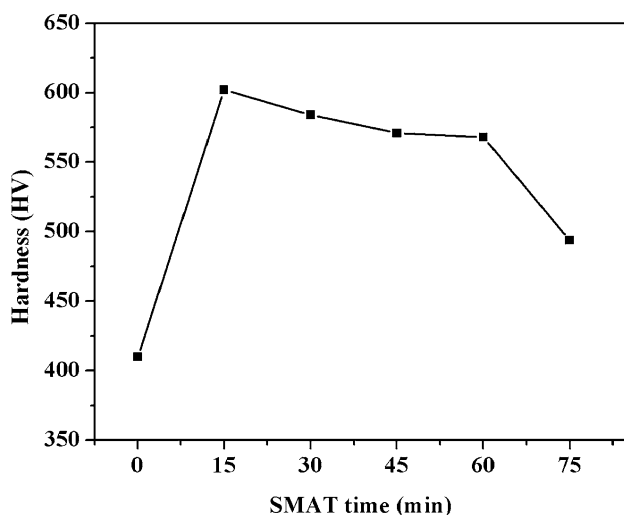


Fig. 15 Surface hardness profiles with SMAT time

## 4 Conclusions

SMAT resulted in mechanically induced tempering of hardened and tempered martensite. The X-ray and microstructural analysis confirmed the formation of carbides indicating the tempering process. Further, it was also noticed that the SMAT produced a composite layer consisting of martensite and carbides. These martensite and carbide phases were refined into finer size and arranged as alternate layers, thereby changing the mechanical properties considerably.

The hardness of mechanically induced tempering processes increased from 400-600 HV<sub>0.2</sub> which was in contrast to a conventional thermal tempering process.

The Young's Modulus increased during the initial process time (15 min) to 40 times and decreased thereafter. This could be attributed to the formation of nano composite layer during the initial stage and formation of surface porosity in later stages.

The yield strength of spring steel increased from 1287 to 1504 MPa, while keeping uniform elongation of 8%.

**Acknowledgements** The authors wish to acknowledge the Director (MANIT Bhopal) for his extensive support. The author is especially grateful to Dr C.M. Krishna for helpful discussions and comments. The author also thanks to Dr. Sanjay Shrivastava (MSME HOD), Dr. O P Modi, BHEL Bhopal and Materials Characterization Lab MME Department for providing their support. The author is grateful for the financial support from MHRD, India.

## References

- Hall E, *Proc Phys Soc Sect B* **64** (1951) 747.
- Petch N, *J Iron Steel Inst* (**174**) 1953 25.
- Lu K, and Lu J, *Mater Sci Eng A* **375** (2004) 38.
- Pedneault S, Huot J, and Roué L, *J Power Source*, **185** (2008) 566.
- Zhang L, et al., *Acta Mater* **49** (2001) 751.
- Zaluski L, Zaluska A, and Ström-Olsen J, *J Alloys Compd* **217** (1995) 245.
- Zaluska A, Zaluski L, and Ström-Olsen J, *J Alloys Compd* **288** (1999) 217.
- Gleiter H, *Progr Mater Sci* **33** (1989) 223.
- Lu K, *Mater Sci Eng R Rep* **16** (1996) 161.
- Suryanarayana C, *Int Mater Rev* **40** (1995) 41.
- Fecht H, et al., *Metall Mater Trans A* **21** (1990) 2333.
- Yin J, Umamoto M, and Tsuchiya K, *ISIJ Int* **41** (2001) 1389.
- Valiev R, Korznikov A, and Mulyukov R, *Mater Sci Eng A* **168** (1993) 141.
- Iwahashi Y, et al., *Scr Mater* **35** (1996) 143.
- Zhilyaev A, et al., *Acta Mater* **51** (2003) 753.
- Miura H, et al., *Trans Nonferrous Met Soc China* **20** (2010) 1294.
- Jian L, *J Mater Sci Technol* **15** (1999) 193.
- Lin Y, et al., *Acta Mater* **54** (2006) 5599.
- Tao N, et al., *Acta Mater* **50** (2002) 4603.
- Tao N, Lu J, and Lu K, in *Materials Science Forum*, Trans Tech Publ, Zurich (2008).
- Villegas J, and Shaw L, *Acta Mater* **57** (2009) 5782.

22. Wen M, et al., *Scr Mater* **68** (2013) 499.
23. Chen X, et al., *Scr Mater* **52** (2005) 1039.
24. Roland T, et al., *Scr Mater* **54** (2006) 1949.
25. Roland T, et al., *Mater Sci Eng A* **445** (2007) 281.
26. Wang Y, et al., *Scr Mater* **48** (2003) 1581.
27. Wang Z, et al., *Mater Sci Eng A* **352** (2003) 144.
28. Bagherifard S, et al., *Int J Fatigue* **65** (2014) 64.
29. Bagherifard S. et al., *Mater Des* **45** (2013) 497.
30. Wang Z, Lu J, and Lu K, *Acta Mater* **53** (2015) 2081.
31. Huang R, and Han Y, *Mater Sci Eng C* **33** (2013) 2353.
32. Bagherifard S, and Guagliano M *Eng Fract Mech* **81** (2012) 56.
33. Vielma A, Llaneza V, and Belzunce F, *Surf Coat Technol* **249** (2014) 75.
34. Torres M, and Voorwald H, *Int J Fatigue* **24** (2002) 877.
35. Roberts C, *Trans AIME* **197** (1953) 203.
36. Peyre P. et al., *Mater Sci Eng A* **280** (2000) 294.
37. Mandal A, and Bandyopadhyay T K, *Steel Res Int* **88** (2017).
38. Coble R, and Kingery W, *J Am Ceram Soc* **39** (1956) 377.